

Valley Gapless Semiconductor: Models and Applications

Kok Wai Lee,¹ Pei-Hao Fu,^{2,1,*} Jun-Feng Liu,² Ching Hua Lee,³ and Yee Sin Ang^{1,†}

¹*Science, Mathematics and Technology, Singapore University of Technology and Design, Singapore 487372, Singapore*

²*School of Physics and Materials Science, Guangzhou University, Guangzhou 510006, China*

³*Department of Physics, National University of Singapore, Singapore 117542*

The emerging field of valleytronics harnesses the valley degree of freedom of electrons, akin to how electronic and spintronic devices utilize the charge and spin degrees of freedom of electrons respectively. The engineering of valleytronic devices typically relies on the coupling between valley and other degrees of freedom such as spin, giving rise to valley-spintronics where an external magnetic field manipulates the information stored in valleys. Here, the valley gapless semiconductor is proposed as a potential electrically controlled valleytronic platform because the valley degree of freedom is coupled to the carrier type, i.e., electrons and holes. The valley degree of freedom can be electrically controlled by tuning the carrier type via the device gate voltage. We demonstrate the proposal for realizing a valley gapless semiconductor in the honeycomb lattice with the Haldane and modified Haldane models. The system's valley-carrier coupling is further studied for its transport properties in an all-electrically controlled valley filter device setting. Our work highlights the significance of the valley gapless semiconductor for valleytronic devices.

I. INTRODUCTION

The emerging field of valleytronics [1–5] harnesses the valley degree of freedom of electrons, similar to how electronic and spintronic [6] devices utilize the charge and spin degrees of freedom of electrons [5] respectively. Valleytronic devices are found in materials such as AlAs [7–9], ferrovalley materials [10–13], transition metal dichalcogenide (TMDC) monolayers [14–24] and bilayer systems [25–33]. Such materials exhibit band structures with two distinct local extrema in the first Brillouin zone, representing degenerate and nonequivalent valleys. The significant separation between valleys effectively suppresses their interaction [34–36], thus making the valley index an independent degree of freedom similar to the internal degrees of freedom of electrons. This unique feature opens up vast possibilities for functional valleytronic devices capable of storing and processing digital information via selective manipulation of electron occupation in specific valleys which have potential applications in quantum computation [25], reversible logic circuits [37], low-power neuromorphic computing [38], thermoelectric materials [39], supercurrent [40–42], Cooper pair splitter [43] and other novel devices [44–48].

The key challenge to designing valleytronic devices involves generating and manipulating valley-polarized carriers. The degeneracy of the two valleys, protected by both the time-reversal and inversion symmetries, limits their direct application in information storage. To address this limitation, methods have been proposed to break the inversion symmetry and induce a valley Hall effect [49] and a valley-polarized quantum anomalous Hall effect [50–53], accumulating valley-polarized carriers perpendicular to an external in-plane electric field. In zigzag

graphene nanoribbons, the unique edge state property enables the proposal of a valley filter and valley valve where the gates in the point contact control the longitudinal edge current polarization [54]. Recent studies on TMDC monolayers also have demonstrated valley-spin coupling due to the broken inversion symmetry [17]. This allows an indirect manipulation of valley-polarized carriers via external fields such as circularly polarized optical excitation [14–16], magnetic fields and proximity effects [17–21, 24]. In bilayer systems, the valley-layer coupling allows electrically controlled valley polarization [28, 32, 33]. Out-of-plane electric polarization or external electric fields can disrupt valley degeneracy in different layers which facilitates electrically controlled valley polarization.

Based on the proposed spin gapless semiconductors [55], the recent concept of the valley gapless semiconductor (VGS) offers another viable approach to manipulating valley-polarized carriers [56]. Generally, the VGS consists of two types. The first type is characterized by a gapless dispersion in one valley and a semiconducting dispersion in the other valley, leading to valley polarization within the semiconducting gap. On the other hand, the second type is characterized by the touching between the conduction band edge of one valley and the valence band edge of the other valley at the Fermi level. Here, we focus on the latter where the valley degree of freedom is coupled to the carrier type. As a result, the electron carriers are contributed by one valley whereas the hole carriers are contributed by the other valley. This unique valley-carrier coupling enables the VGS to serve as a potential platform for electrically controlled valleytronics.

In this work, we introduce the concept of the VGS via a two-band Dirac-type Hamiltonian where a valley-dependent scalar potential term induces the VGS by shifting the energies of the Dirac points. We further demonstrate its realization in the honeycomb lattice where its emergence is governed by the competition between the Haldane [57] and modified Haldane terms [58].

* phy.phfu@gmail.com

† yeesin_ang@sutd.edu.sg

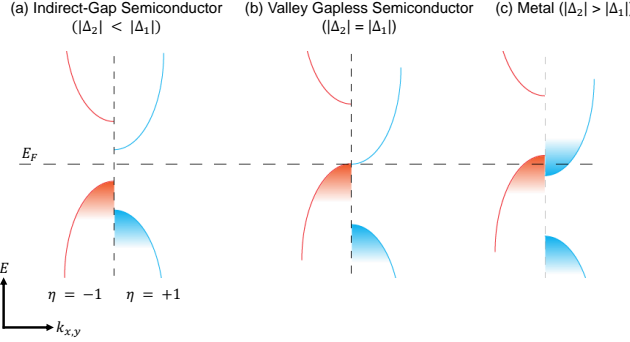


FIG. 1. Schematic of the band structure of the (a) indirect-gap semiconductor with $|\Delta_2| < |\Delta_1|$, (b) valley gapless semiconductor with $|\Delta_2| = |\Delta_1|$ and (c) metal with $|\Delta_2| > |\Delta_1|$.

Appropriate parameter choices lead to the coupling between the valley degree of freedom and carrier type, paving the way for valleytronic device applications. To this end, we characterize its transport properties in an all-electrically controlled valley filter device setting by computing the valley-dependent conductance and valley polarization efficiency.

The remainder of this paper is organized as follows. In Sec. II, we introduce the concept of the VGS and discuss its characteristics. Sec. III presents the model for the VGS in the honeycomb lattice. In Sec. IV, we delve into all-electrically controlled valleytronics, focusing on the valley filter. Finally, the results are summarized in Sec. V.

II. VALLEY GAPLESS SEMICONDUCTOR

We demonstrate the concept of a two-dimensional VGS via the following two-band valley-dependent Dirac-type Hamiltonian:

$$\mathcal{H}_\eta(\mathbf{k}) = \eta \hbar v_{F_x} k_x \tau_x + \hbar v_{F_y} k_y \tau_y - \Delta_1 \tau_z - \eta \Delta_2 \tau_0, \quad (1)$$

where $\mathbf{k} = (k_x, k_y)$, $\eta = \pm 1$ denotes the valley index, $v_{F_x(y)}$ is the Fermi velocity along the $x(y)$ -direction and τ (τ_0) is the Pauli (unit) matrix of the sublattice pseudospin. The last two terms are the Dirac mass term, Δ_1 and valley-dependent scalar potential, Δ_2 which shift the energies of the Dirac points. Here, we assume that the inter-valley interaction is negligible.

The competition between Δ_1 and Δ_2 is crucial for determining the phases of the system as indicated by the following eigenvalues of Eq. (1):

$$E_{\eta,\pm}(\mathbf{k}) = -\eta \Delta_2 \pm \sqrt{(\hbar v_F |\mathbf{k}|)^2 + \Delta_1^2}. \quad (2)$$

For $\Delta_1 = \Delta_2 = 0$, the system is gapless which is known as a Dirac semimetal, supporting two Dirac points localized at the same energy. When $\Delta_1 \neq 0$, the Dirac

points are destroyed and the band structures illustrated in Fig. 1 reveal an intravalley gap, denoted as Δ_{intra} , which represents the energy difference between the conduction and valence band edges within each individual valley. The intravalley gap is related to the Dirac mass term via

$$\Delta_{intra} = |E_{\eta,+} - E_{\eta,-}| = 2 |\Delta_1|. \quad (3)$$

The system manifests a semiconducting phase when the Fermi level lies within this gap.

When both Δ_1 and $\Delta_2 \neq 0$, the system's classification as a semiconductor or a metal depends on the relative strength between Δ_1 and Δ_2 . In this regard, an intervalley gap, denoted as Δ_{inter} , is defined to be the minimum energy difference between the edges of the conduction band in one valley and the valence band in the other valley which is expressed as

$$\Delta_{inter} = \min [\Delta_+, \Delta_-], \quad (4)$$

where

$$\Delta_\eta = E_{\eta,+} - E_{\bar{\eta},-} = 2 (|\Delta_1| - \eta \Delta_2), \quad (5)$$

and $\bar{\eta} = -\eta$. When $|\Delta_2| < |\Delta_1|$, the system is an indirect-gap semiconductor [Fig. 1(a)] with both non-zero intravalley gap ($\Delta_{intra} \neq 0$) and intervalley gap ($\Delta_{inter} > 0$). On the other hand, the system becomes metallic when $|\Delta_2| > |\Delta_1|$ even if an indirect gap between the valleys exists [Fig. 1(c)] because it is now negative ($\Delta_{inter} < 0$). In the regime of $|\Delta_2| - |\Delta_1| < E < |\Delta_2| + |\Delta_1|$ and $-(|\Delta_2| + |\Delta_1|) < E < |\Delta_1| - |\Delta_2|$, the system is of valley-half-metallic feature, the electrons and holes are contributed by the $\eta = +1$ (-1) and $\eta = -1$ ($+1$) valleys for positive (negative) Δ_2 respectively. This phase resembles a spinful half-metal in ferromagnets where the carrier is contributed by one of the spin subbands.

At $|\Delta_2| = |\Delta_1|$, the intervalley gap vanishes ($\Delta_{inter} = 0$). Consequently, this critical phase between the two aforementioned phases is dubbed as the VGS. For $-2|\Delta_1| < E < 2|\Delta_1|$, the charge carriers are valley-polarized. Similar to the spin gapless semiconductor, the VGS supports electrons with $\eta = +1$ (-1) valley polarization and holes with $\eta = -1$ ($+1$) valley polarization for positive (negative) Δ_2 respectively. The VGS, being characterized by a continuous energy distribution of valley-polarized charge carriers as compared to the indirect-gap semiconducting and metallic phases, exhibits potential applications in electrically controlled valleytronics.

III. VGS REALIZATION IN THE HONEYCOMB LATTICE

We demonstrate the realization of the VGS, semiconducting and metallic phases in the honeycomb lattice subject to the Haldane and modified Haldane terms

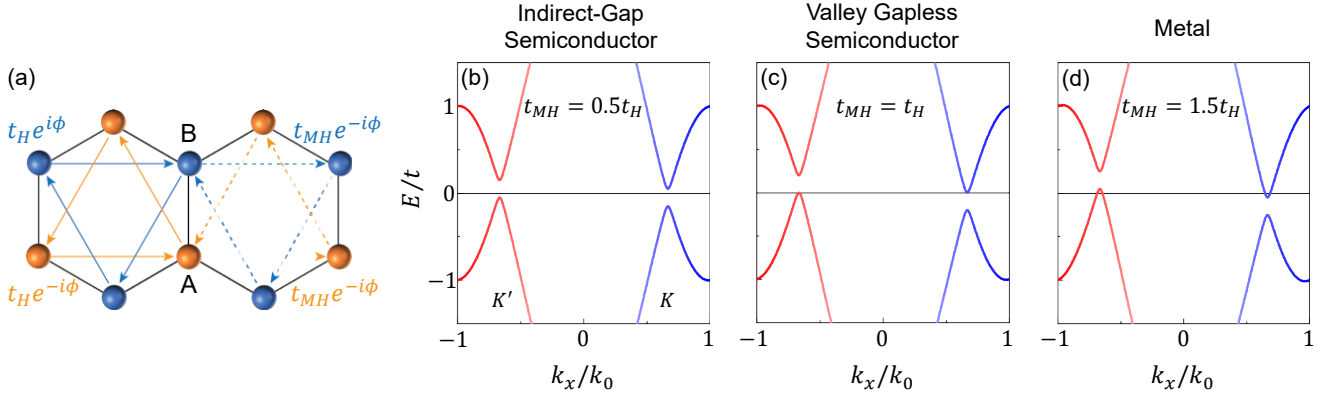


FIG. 2. (a) Schematic of the Haldane (t_H) and modified Haldane (t_{MH}) next-nearest-neighbour hoppings where their competition determines the phase of the system, i.e., (b) indirect-gap semiconductor when $t_{MH} < t_H$, (c) valley gapless semiconductor when $t_{MH} = t_H$ and (d) metal when $t_{MH} > t_H$. For (b) to (d), the Haldane hopping strength is set at $t_H = 0.1t$ where the nearest-neighbor hopping strength serves as the energy unit ($t = 1$). The unit of k_x is $k_0 = 2\pi/\sqrt{3}a$ where a is the graphene lattice constant taken to be 1.

[58, 59] [Fig. 2(a)] which is described by the following Hamiltonian:

$$\mathcal{H}_{hc} = -t \sum_{\langle i,j \rangle} c_i^\dagger c_j + \frac{1}{3\sqrt{3}} \sum_{\langle\langle i,j \rangle\rangle} \left(t_{H} e^{-iv_{ij}\phi} + t_{MH} e^{-iv'_{ij}\phi'} \right) c_i^\dagger c_j + H.c. \quad (6)$$

Here, $c_i^\dagger (c_i)$ is the spinless fermionic creation (annihilation) operator acting at the i th site, the summation of $\langle ij \rangle$ ($\langle\langle ij \rangle\rangle$) runs over all the nearest (next-nearest)-neighbor sites and $H.c.$ denotes the Hermitian conjugate. The first term describes the nearest-neighbor hopping with strength t . The second term describes the Haldane (modified Haldane) next-nearest-neighbor hopping with strength t_H (t_{MH}) [57, 58]. $v_{ij} = +1$ (-1) denotes the counterclockwise (clockwise) hopping for both sublattices A and B. On the other hand, $v'_{ij} = \pm 1$ ($v'_{ij} = \mp 1$) for sublattice A (B) as illustrated in Fig. 2(a). The competition between the Haldane and modified Haldane terms determines the emergence of the VGS.

The electronic states in the vicinity of the $\mathbf{K}_{\eta=\pm 1} = [\eta 4\pi/(3\sqrt{3}a), 0]$ points are described by the following low-energy effective Hamiltonian:

$$\mathcal{H}_{hc}^\eta(\mathbf{k}) = \mathcal{H}_\eta(\mathbf{k}) - \frac{1}{\sqrt{3}} (t_H \cos \phi + t_{MH} \cos \phi') \tau_0, \quad (7)$$

where $\hbar v_{F_x} = \hbar v_{F_y} = 3t/2a$ ($a = 1$ is the graphene lattice constant), $\Delta_1 = \eta t_H \sin \phi$, $\Delta_2 = t_{MH} \sin \phi'$, and τ (τ_0) is the Pauli (unit) matrix of the sublattice pseudospin. For $\phi = 0$ or $\phi' = 0$, the two Haldane terms behave as conventional next-nearest-neighbor hopping terms which shift the two Dirac cones equally in energy scale. We focus on the case where $\phi = \phi' = \pi/2$ and we also assume that both t_H and $t_{MH} > 0$ without loss of generality. In this case, the modified Haldane term is also

known as the staggered Haldane term [60] which breaks the time-reversal symmetry but preserves the sublattice pseudospin symmetry. Therefore, the modified Haldane term induces a valley-dependent scalar potential shifting the energies of the Dirac cones [58], which is necessary to realize the VGS and the other two phases.

Following the discussion in Sec. II, the VGS occurs when $\Delta_{intra} = 2|\Delta_1| = 2t_H \neq 0$ and $\Delta_{inter} = 2(t_H - t_{MH}) = 0$ or $t_H = t_{MH}$. On the other hand, the indirect-gap semiconducting and metallic phases are obtained when $t_{MH} < t_H$ and $t_{MH} > t_H$ respectively as depicted in Figs. 2 (b) to (d).

The Haldane model has been experimentally realized via ultracold atoms in an optical lattice [61], AB-stacked MoTe₂/WSe₂ moiré bilayers [62], light-wave-controlled monolayer hexagonal boron nitride [63] and monolayer graphene optically driven by a circularly polarized light [64, 65]. Meanwhile, the experimental realization of the modified Haldane model is possible in artificial systems such as a microwave-scale gyromagnetic photonic crystal [66], topological circuit [67], 3D layer-stacked photonic metacrystal [68] and magnetic Weyl photonic crystal [69] as well as ferromagnet/graphene/TMDC heterostructures [10, 58, 59, 70, 71]. In particular, in TMDC monolayers such as MoS₂ [24, 58], the VGS is expected in one of the spin sub-bands because the spin-orbit coupling produces both the Haldane and modified Haldane terms.

IV. VALLEY FILTER

In this section, we investigate the valley-filter effect of the VGS, semiconducting and metallic phases as a means to generate valley-polarized carriers. In particular, since the electrons and holes in the VGS are bound to different valleys, naturally such a VGS-based valley filter is

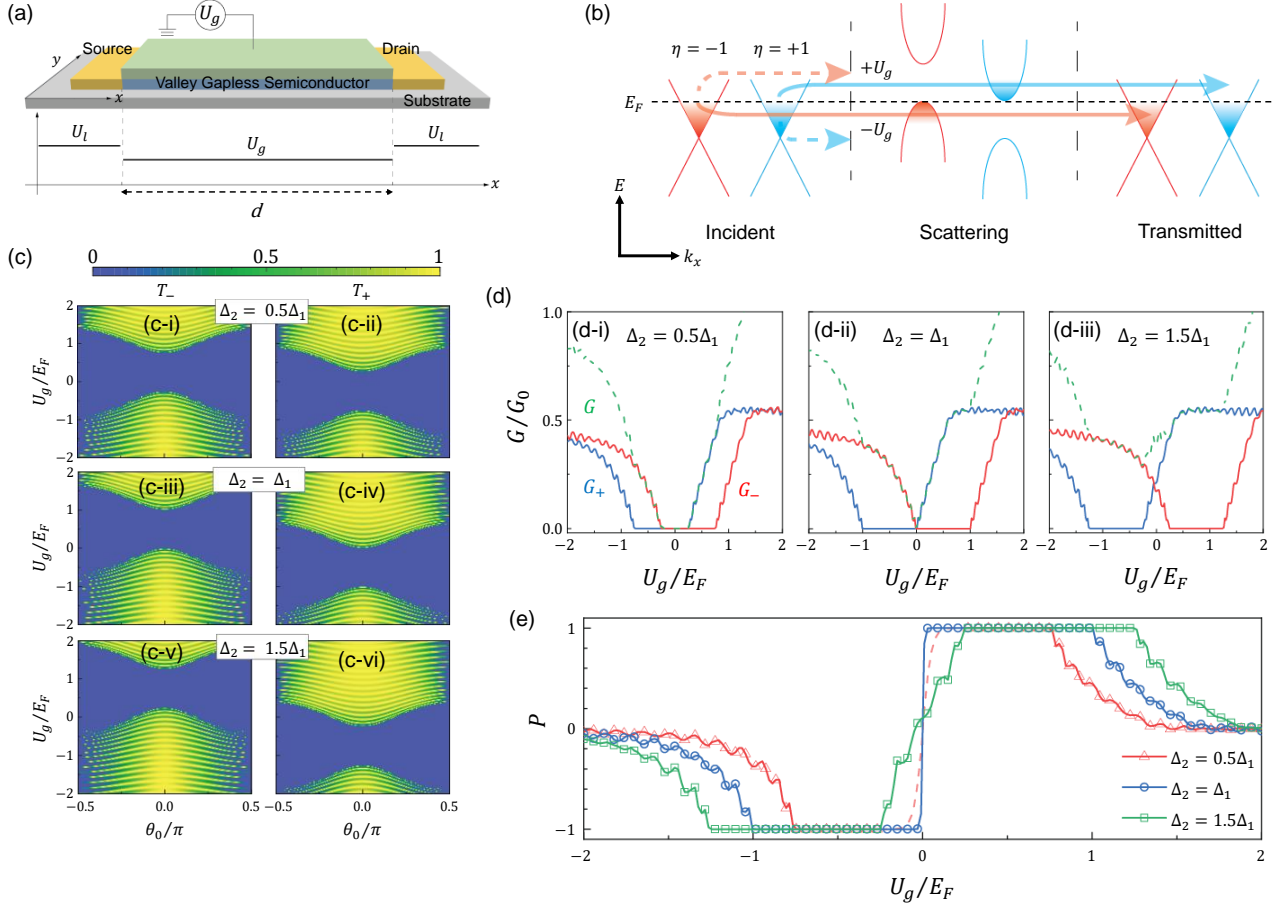


FIG. 3. (a) Schematic of the gate-controlled VGS-based valley filter where the gate voltage, U_g is applied to the central region with length, d . (b) The mechanism of the gate-controlled valley-filter effect. For a positive (negative) gate voltage, only the electrons (holes) in the $\eta = +1$ (-1) valley are transmitted because of the VGS. (c) The valley-dependent transmission probability, T_η with respect to the gate voltage, U_g (in the unit of the Fermi level, E_F) and the incident direction of the electrons, θ_0 . The left (right) panels depict the transmission probability of the $\eta = -1$ ($+1$) valley for various values of Δ_1 and Δ_2 . The top, middle and bottom panels refer to the indirect-gap semiconducting, VGS and metallic phases with $\Delta_2 = 0.5\Delta_1$, $\Delta_2 = \Delta_1$ and $\Delta_2 = 1.5\Delta_1$ respectively. The gate-controlled (d) conductance, G and (e) valley polarization efficiency, P of the three phases. The conductance is shown in the unit of $G_0 = e^2/W\hbar$ with sample width, W . The red dashed line in (e) indicates the ill-defined P due to the vanishing conductance. $E_F = 1$ is chosen as the energy unit and the system is isotropic with $\hbar v_{F_x} k_F = \hbar v_{F_y} k_F = 1$. In the central region, $\Delta_1 = 0.5E_F$ whereas the length is $k_F d = 20$.

electrically manipulable. The device [Fig. 3(a)] can be constructed by sandwiching a VGS between two normal metallic leads acting as the source and drain without any valley nonequivalence. The central region is controlled by a top gate. Figure 3(b) illustrates the all-gate tunable feature of the VGS-based valley filter device.

Considering that the system is translationally invariant in the y -direction, i.e., k_y is a good quantum number, the corresponding Hamiltonian is

$$\mathcal{H}_1^\eta(x, k_y) = \mathcal{H}^\eta(-i\partial_x, k_y) - U(x)\tau_0, \quad (8)$$

with $\Delta_{1,2}(x) = \Delta_{1,2}\Theta(dx - x^2)$ and $U(x) = U_l\Theta(-x) + U_g\Theta(dx - x^2) + U_l\Theta(x - d)$, where U_l is the electrostatic potential in the leads and the VGS is confined within the

central region of length, d and manipulated by the gate voltage, U_g .

The valley-filter effect manifests as the valley-dependent transmission probability, $T_\eta = |t_\eta|^2$ obtained by matching the wavefunctions

$$\psi_\eta(x) = \begin{cases} \psi_\eta^+(x) + r_\eta \psi_\eta^-(x), & x < 0 \\ a\psi_\eta^+(x) + b\psi_\eta^-(x), & 0 \leq x \leq d \\ t_\eta \psi_\eta^+(x), & x > d \end{cases}, \quad (9)$$

at $x = 0$ and $x = d$ where

$$\psi_\eta^\pm(x) = \begin{pmatrix} \pm\eta e^{\mp i\eta\theta(x)} \\ S(x)\gamma(x) \end{pmatrix} e^{\pm ik(x)x} e^{ik_y y}, \quad (10)$$

is the wavefunction of the three regions characterized

by $\hbar v_{F_x} k(x) = \pm \sqrt{Z_+(x) Z_-(x) - (\hbar v_{F_y} k_y)^2}$, $\gamma(x) = \sqrt{1 - 2\Delta_1(x)/Z_+(x)}$, $S(x) = \text{sign}(Z_-)$, $\theta(x) = \arctan[v_{F_x} k(x)/v_{F_y} k_y]$ and $Z_{\pm}(x) = E + U(x) + \eta\Delta_2(x) \pm \Delta_1(x)$ where E is the energy of the incident electrons.

At $T = 0$, the valley-dependent conductance is related to the transmission probability as

$$G_{\eta}(E_F)/G_0 = \int_{-\pi/2}^{\pi/2} T_{\eta}(E_F, \theta_0) \cos \theta_0 d\theta_0, \quad (11)$$

where $\theta_0 = \arcsin(\hbar v_{F_y} k_y / E_F^{1/2})$ and $E_F = U_l + E$ are the direction and Fermi level of the incident electrons respectively. The conductance is normalized by the conductance unit, $G_0 = e^2/W\hbar$ with sample width, W .

Hereafter, $E_F = 1$ is chosen as the energy unit and the system is isotropic with $\hbar v_{F_x} k_F = \hbar v_{F_y} k_F = 1$. In the central region, $\Delta_1 = 0.5E_F$ whereas the length is $k_F d = 20$. We argue that the results below are qualitatively similar for different combinations of the parameters.

To demonstrate the valley-filter effect, we first obtain the valley-dependent transmission probability, T_{η} with respect to the incident direction of the electrons, θ_0 and gate voltage, U_g of the indirect-gap semiconducting ($\Delta_2 = 0.5\Delta_1$), VGS ($\Delta_2 = \Delta_1$) and metallic ($\Delta_2 = 1.5\Delta_1$) phases [Fig. 3(c)]. For all three phases, the transmission coefficient vanishes beyond a critical angle, $\theta_{\eta}^c = \arcsin[\sqrt{Z_+(d)Z_-(d)}/E_F]$. Electrons with incident angle beyond θ_{η}^c are reflected completely due to the evanescent wave in the central region. Moreover, the transmission probability vanishes when the gate voltage within the band gap of each valley, i.e., $-(\eta\Delta_2 + \Delta_1) < U_g < -(\eta\Delta_2 - \Delta_1)$, is swept. However, this voltage window is valley-dependent due to the energy shifting of the Dirac cones by Δ_2 which results in carriers being valley-selectively transmitted. By tuning the gate voltage, only carriers from one valley are allowed to be transmitted whereas the transmission of carriers from the other valley is forbidden as illustrated schematically in Fig. 3(b). Therefore, the total conductance, $G = G_+ + G_-$ within this regime is solely contributed by carriers from one valley only, i.e., either $G = G_+$ or $G = G_-$ as shown in Fig. 3(d). Beyond this voltage window, the conductance contribution from the other valley increases gradually and the total conductance oscillates due to Fabry-Pérot interference.

The valley-filter effect is characterized in terms of the valley polarization efficiency defined as

$$P = \frac{G_+ - G_-}{G_+ + G_-}. \quad (12)$$

Figure 3(e) depicts the valley polarization efficiency, P with respect to the gate voltage, U_g of the three phases. For each of them, a full valley polarization efficiency of $P = -1$ (+1) is achieved when the gate voltage satisfies $-(\Delta_2 + \Delta_1) < U_g < \Delta_1 - \Delta_2$ ($\Delta_2 - \Delta_1 < U_g < \Delta_2 + \Delta_1$).

The valley polarization efficiency is destroyed gradually when the gate voltage exceeds the aforementioned range of values. In particular, the VGS ($\Delta_2 = \Delta_1$) experiences a sharp flip of the valley polarization efficiency between $P = -1$ and $P = +1$ at $U_g = 0$ [Fig. 3(e)] owing to the valley-carrier coupling. Hence, its conductance is solely contributed by electrons from the $\eta = -1$ (+1) valley when $U_g < 0$ ($U_g > 0$). On the other hand, the valley polarization efficiency of the semiconducting phase ($\Delta_2 < \Delta_1$) is ill-defined for $|U_g| < \Delta_1 - \Delta_2$ [red dashed line in Fig. 3(e)] due to the vanishing conductance [Fig. 3(d-i)]. For the metallic phase ($\Delta_2 > \Delta_1$), its valley polarization efficiency is unstable and sensitive to the gate voltage. The results demonstrate that the VGS phase is well suited for a valley filter device owing to the valley-carrier coupling.

V. CONCLUSION

In summary, we have theoretically investigated a VGS-based valleytronic device where its valley-carrier coupling feature enables a fully valley-polarized current with all-electrical manipulation. A possible realization scheme of the VGS phase is demonstrated in the honeycomb lattice subject to the Haldane and modified Haldane terms. The Haldane terms have been experimentally realized in many systems including light-wave-controlled monolayer hexagonal boron nitride [63], optically driven monolayer graphene [64, 65], topological circuit [67] and magnetic Weyl photonic crystal [69]. Furthermore, the valley-filter effect of the VGS phase is studied in a single gate-controlled valley filter device where it manifests a sharp flip of the valley polarization efficiency between $P = -1$ and $P = +1$ at $U_g = 0$ due to the valley-carrier coupling. This highlights the potential application of the VGS phase in valleytronics including valley-based quantum computing and improving classical information storage and processing [72]. It is possible to realize the VGS phase in other lattice systems such as the square [73], $\alpha - T_3$ [74, 75] and dice [76, 77] lattices, subject not only to the Haldane and modified Haldane terms, but also other effects such as Floquet driving [78–80], strain engineering [81] and spin-orbit coupling effects [82–85].

ACKNOWLEDGMENTS

K. W. Lee is supported by the SUTD PhD Scholarship. P.-H. Fu & Y. S. Ang are supported by the Singapore Ministry of Education (MOE) Academic Research Fund (AcRF) Tier 2 Grant (MOE-T2EP50221-0019). J.-F. L. is supported by the National Natural Science Foundation of China (Grant No. 12174077). C. H. L. is supported by Singapore's NRF Quantum Engineering grant NRF2021-QEP2-02-P09 and Singapore's MOE Tier-II grant Proposal ID: T2EP50222-0003.

[1] J.-D. Zheng, Y.-F. Zhao, Y.-F. Tan, Z. Guan, N. Zhong, F.-Y. Yue, P.-H. Xiang, and C.-G. Duan, Coupling of ferroelectric and valley properties in 2D materials, *J. Appl. Phys.* **132**, 120902 (2022).

[2] Y. Liu, Y. Gao, S. Zhang, J. He, J. Yu, and Z. Liu, Valleytronics in transition metal dichalcogenides materials, *Nano Res.* **12**, 2695 (2019).

[3] J. R. Schaibley, H. Yu, G. Clark, P. Rivera, J. S. Ross, K. L. Seyler, W. Yao, and X. Xu, Valleytronics in 2D materials, *Nat Rev Mater* **1**, 1 (2016).

[4] H. Yu, X. Cui, X. Xu, and W. Yao, Valley excitons in two-dimensional semiconductors, *Natl. Sci. Rev.* **2**, 57 (2015).

[5] X. Xu, W. Yao, D. Xiao, and T. F. Heinz, Spin and pseudospins in layered transition metal dichalcogenides, *Nature Phys* **10**, 343 (2014).

[6] I. Žutić, J. Fabian, and S. Das Sarma, Spintronics: Fundamentals and applications, *Rev. Mod. Phys.* **76**, 323 (2004).

[7] O. Gunawan, Y. P. Shkolnikov, K. Vakili, T. Gokmen, E. P. De Poortere, and M. Shayegan, Valley Susceptibility of an Interacting Two-Dimensional Electron System, *Phys. Rev. Lett.* **97**, 186404 (2006).

[8] T. Gokmen, M. Padmanabhan, O. Gunawan, Y. P. Shkolnikov, K. Vakili, E. P. De Poortere, and M. Shayegan, Parallel magnetic-field tuning of valley splitting in AlAs two-dimensional electrons, *Phys. Rev. B* **78**, 233306 (2008).

[9] M. A. Mueed, M. S. Hossain, I. Jo, L. N. Pfeiffer, K. W. West, K. W. Baldwin, and M. Shayegan, Realization of a Valley Superlattice, *Phys. Rev. Lett.* **121**, 036802 (2018).

[10] W.-Y. Tong, S.-J. Gong, X. Wan, and C.-G. Duan, Concepts of ferrovalley material and anomalous valley Hall effect, *Nat Commun* **7**, 13612 (2016).

[11] X.-W. Shen, W.-Y. Tong, S.-J. Gong, and C.-G. Duan, Electrically tunable polarizer based on 2D orthorhombic ferrovalley materials, *2D Mater.* **5**, 011001 (2017).

[12] Y. Lai, Z. Song, Y. Wan, M. Xue, C. Wang, Y. Ye, L. Dai, Z. Zhang, W. Yang, H. Du, *et al.*, Two-dimensional ferromagnetism and driven ferroelectricity in van der Waals CuCrP 2 S 6, *Nanoscale* **11**, 5163 (2019).

[13] H. Hu, W.-Y. Tong, Y.-H. Shen, X. Wan, and C.-G. Duan, Concepts of the half-valley-metal and quantum anomalous valley Hall effect, *npj Comput Mater* **6**, 129 (2020).

[14] T. Cao, G. Wang, W. Han, H. Ye, C. Zhu, J. Shi, Q. Niu, P. Tan, E. Wang, B. Liu, *et al.*, Valley-selective circular dichroism of monolayer molybdenum disulphide, *Nat Commun* **3**, 887 (2012).

[15] H. Zeng, J. Dai, W. Yao, D. Xiao, and X. Cui, Valley polarization in MoS2 monolayers by optical pumping, *Nature Nanotech* **7**, 490 (2012).

[16] A. M. Jones, H. Yu, N. J. Ghimire, S. Wu, G. Aivazian, J. S. Ross, B. Zhao, J. Yan, D. G. Mandrus, D. Xiao, *et al.*, Optical generation of excitonic valley coherence in monolayer WSe2, *Nature Nanotech* **8**, 634 (2013).

[17] R. Suzuki, M. Sakano, Y. Zhang, R. Akashi, D. Morikawa, A. Harasawa, K. Yaji, K. Kuroda, K. Miyamoto, T. Okuda, *et al.*, Valley-dependent spin polarization in bulk MoS2 with broken inversion symmetry, *Nature Nanotech* **9**, 611 (2014).

[18] G. Aivazian, Z. Gong, A. M. Jones, R.-L. Chu, J. Yan, D. G. Mandrus, C. Zhang, D. Cobden, W. Yao, and X. Xu, Magnetic control of valley pseudospin in monolayer WSe2, *Nature Phys* **11**, 148 (2015).

[19] Z. Wang, J. Shan, and K. F. Mak, Valley-and spin-polarized Landau levels in monolayer WSe2, *Nature Nanotech* **12**, 144 (2017).

[20] D. Zhong, K. L. Seyler, X. Linpeng, R. Cheng, N. Sivadas, B. Huang, E. Schmidgall, T. Taniguchi, K. Watanabe, M. A. McGuire, W. Yao, D. Xiao, K.-M. C. Fu, and X. Xu, Van der Waals engineering of ferromagnetic semiconductor heterostructures for spin and valleytronics, *Sci. Adv.* **3**, e1603113 (2017).

[21] P. Dey, L. Yang, C. Robert, G. Wang, B. Urbaszek, X. Marie, and S. A. Crooker, Gate-Controlled Spin-Valley Locking of Resident Carriers in WSe2 Monolayers, *Phys. Rev. Lett.* **119**, 137401 (2017).

[22] Z. Wu, B. T. Zhou, X. Cai, P. Cheung, G.-B. Liu, M. Huang, J. Lin, T. Han, L. An, Y. Wang, *et al.*, Intrinsic valley Hall transport in atomically thin MoS2, *Nat Commun* **10**, 611 (2019).

[23] L. Li, L. Shao, X. Liu, A. Gao, H. Wang, B. Zheng, G. Hou, K. Shehzad, L. Yu, F. Miao, *et al.*, Room-temperature valleytronic transistor, *Nat. Nanotechnol.* **15**, 743 (2020).

[24] D. Xiao, G.-B. Liu, W. Feng, X. Xu, and W. Yao, Coupled Spin and Valley Physics in Monolayers of MoS2 and Other Group-VI Dichalcogenides, *Phys. Rev. Lett.* **108**, 196802 (2012).

[25] Z. Gong, G.-B. Liu, H. Yu, D. Xiao, X. Cui, X. Xu, and W. Yao, Magnetoelectric effects and valley-controlled spin quantum gates in transition metal dichalcogenide bilayers, *Nat Commun* **4**, 2053 (2013).

[26] S. Wu, J. S. Ross, G.-B. Liu, G. Aivazian, A. Jones, Z. Fei, W. Zhu, D. Xiao, W. Yao, D. Cobden, *et al.*, Electrical tuning of valley magnetic moment through symmetry control in bilayer MoS2, *Nature Phys* **9**, 149 (2013).

[27] A. M. Jones, H. Yu, J. S. Ross, P. Klement, N. J. Ghimire, J. Yan, D. G. Mandrus, W. Yao, and X. Xu, Spin-layer locking effects in optical orientation of exciton spin in bilayer WSe2, *Nature Phys* **10**, 130 (2014).

[28] M. Sui, G. Chen, L. Ma, W.-Y. Shan, D. Tian, K. Watanabe, T. Taniguchi, X. Jin, W. Yao, D. Xiao, *et al.*, Gate-tunable topological valley transport in bilayer graphene, *Nature Phys* **11**, 1027 (2015).

[29] Y. Shimazaki, M. Yamamoto, I. V. Borzenets, K. Watanabe, T. Taniguchi, and S. Tarucha, Generation and detection of pure valley current by electrically induced Berry curvature in bilayer graphene, *Nature Phys* **11**, 1032 (2015).

[30] J. Lee, K. F. Mak, and J. Shan, Electrical control of the valley Hall effect in bilayer MoS2 transistors, *Nature Nanotech* **11**, 421 (2016).

[31] G. Scuri, T. I. Andersen, Y. Zhou, D. S. Wild, J. Sung, R. J. Gelly, D. Bérubé, H. Heo, L. Shao, A. Y. Joe, A. M. Mier Valdivia, T. Taniguchi, K. Watanabe, M. Lončar, P. Kim, M. D. Lukin, and H. Park, Electrically Tunable Valley Dynamics in Twisted WSe2/WSe2 Bilayers, *Phys. Rev. Lett.* **124**, 217403 (2020).

[32] Z.-M. Yu, S. Guan, X.-L. Sheng, W. Gao, and S. A. Yang, Valley-Layer Coupling: A New Design Principle for Val-

leytronics, *Phys. Rev. Lett.* **124**, 037701 (2020).

[33] T. Zhang, X. Xu, B. Huang, Y. Dai, L. Kou, and Y. Ma, Layer-polarized anomalous Hall effects in valleytronic van der Waals bilayers, *Mater. Horiz.* **10**, 483 (2023).

[34] E. McCann, K. Kechedzhi, V. I. Fal'ko, H. Suzuura, T. Ando, and B. L. Altshuler, Weak-Localization Magnetoresistance and Valley Symmetry in Graphene, *Phys. Rev. Lett.* **97**, 146805 (2006).

[35] S. V. Morozov, K. S. Novoselov, M. I. Katsnelson, F. Schedin, L. A. Ponomarenko, D. Jiang, and A. K. Geim, Strong Suppression of Weak Localization in Graphene, *Phys. Rev. Lett.* **97**, 016801 (2006).

[36] A. F. Morpurgo and F. Guinea, Intervalley Scattering, Long-Range Disorder, and Effective Time-Reversal Symmetry Breaking in Graphene, *Phys. Rev. Lett.* **97**, 196804 (2006).

[37] Y. S. Ang, S. A. Yang, C. Zhang, Z. Ma, and L. K. Ang, Valleytronics in merging Dirac cones: All-electric-controlled valley filter, valve, and universal reversible logic gate, *Phys. Rev. B* **96**, 245410 (2017).

[38] J. Chen, Y. Zhou, J. Yan, J. Liu, L. Xu, J. Wang, T. Wan, Y. He, W. Zhang, and Y. Chai, Room-temperature valley transistors for low-power neuromorphic computing, *Nat. Commun.* **13**, 7758 (2022).

[39] J. Xin, Y. Tang, Y. Liu, X. Zhao, H. Pan, and T. Zhu, Valleytronics in thermoelectric materials, *npj Quant Mater* **3**, 9 (2018).

[40] Y.-M. Xie, D. K. Efetov, and K. T. Law, φ_0 -Josephson junction in twisted bilayer graphene induced by a valley-polarized state, *Phys. Rev. Res.* **5**, 023029 (2023).

[41] C. W. J. Beenakker, N. V. Gnezdilov, E. Dresselhaus, V. P. Ostroukh, Y. Herasymenko, i. d. I. Adagideli, and J. Tworzydło, Valley switch in a graphene superlattice due to pseudo-Andreev reflection, *Phys. Rev. B* **97**, 241403 (2018).

[42] J. J. Wang, S. Liu, J. Wang, and J.-F. Liu, Valley supercurrent in the Kekulé graphene superlattice heterojunction, *Phys. Rev. B* **101**, 245428 (2020).

[43] X. Wu, H. Meng, F. Kong, H. Zhang, Y. Bai, and N. Xu, Tunable nonlocal valley-entangled Cooper pair splitter realized in bilayer-graphene van der Waals spin valves, *Phys. Rev. B* **101**, 125406 (2020).

[44] X. Chen, L. Zhang, and H. Guo, Valley caloritronics and its realization by graphene nanoribbons, *Phys. Rev. B* **92**, 155427 (2015).

[45] X.-T. An, J. Xiao, M. W.-Y. Tu, H. Yu, V. I. Fal'ko, and W. Yao, Realization of Valley and Spin Pumps by Scattering at Nonmagnetic Disorders, *Phys. Rev. Lett.* **118**, 096602 (2017).

[46] Z. Wu, F. Zhai, F. M. Peeters, H. Q. Xu, and K. Chang, Valley-Dependent Brewster Angles and Goos-Hänchen Effect in Strained Graphene, *Phys. Rev. Lett.* **106**, 176802 (2011).

[47] X. Qiu, Q. Lv, and Z. Cao, A high-quality spin and valley beam splitter in WSe₂ tunnelling junction through the Goos-Hänchen shift, *J. Phys.: Condens. Matter* **31**, 225303 (2019).

[48] R. Liu, Y. Zhang, Y. Zhou, J. Nie, L. Li, and Y. Zhang, Polarization-driven high Rabi frequency of piezotronic valley transistors, *Nano Energy* **113**, 108550 (2023).

[49] D. Xiao, W. Yao, and Q. Niu, Valley-Contrasting Physics in Graphene: Magnetic Moment and Topological Transport, *Phys. Rev. Lett.* **99**, 236809 (2007).

[50] J. Zhou, Q. Sun, and P. Jena, Valley-Polarized Quantum Anomalous Hall Effect in Ferrimagnetic Honeycomb Lattices, *Phys. Rev. Lett.* **119**, 046403 (2017).

[51] H. Pan, Z. Li, C.-C. Liu, G. Zhu, Z. Qiao, and Y. Yao, Valley-Polarized Quantum Anomalous Hall Effect in Silicene, *Phys. Rev. Lett.* **112**, 106802 (2014).

[52] H. Pan, X. Li, F. Zhang, and S. A. Yang, Perfect valley filter in a topological domain wall, *Phys. Rev. B* **92**, 041404 (2015).

[53] H. Pan, X. Li, H. Jiang, Y. Yao, and S. A. Yang, Valley-polarized quantum anomalous Hall phase and disorder-induced valley-filtered chiral edge channels, *Phys. Rev. B* **91**, 045404 (2015).

[54] A. Rycerz, J. Tworzydło, and C. Beenakker, Valley filter and valley valve in graphene, *Nature Phys.* **3**, 172 (2007).

[55] X. L. Wang, Proposal for a New Class of Materials: Spin Gapless Semiconductors, *Phys. Rev. Lett.* **100**, 156404 (2008).

[56] S.-D. Guo, Y.-L. Tao, G. Wang, S. Chen, D. Huang, and Y. S. Ang, Proposal for valleytronic materials: Ferrovalley metal and valley gapless semiconductor, *Front. Phys.* **19**, 23302 (2024).

[57] F. D. M. Haldane, Model for a Quantum Hall Effect without Landau Levels: Condensed-Matter Realization of the "Parity Anomaly", *Phys. Rev. Lett.* **61**, 2015 (1988).

[58] E. Colomés and M. Franz, Antichiral Edge States in a Modified Haldane Nanoribbon, *Phys. Rev. Lett.* **120**, 086603 (2018).

[59] M. Vila, N. T. Hung, S. Roche, and R. Saito, Tunable circular dichroism and valley polarization in the modified Haldane model, *Phys. Rev. B* **99**, 161404 (2019).

[60] M. Ezawa, Spin valleytronics in silicene: Quantum spin Hall-quantum anomalous Hall insulators and single-valley semimetals, *Phys. Rev. B* **87**, 155415 (2013).

[61] G. Jotzu, M. Messer, R. Desbuquois, M. Lebrat, T. Uehlinger, D. Greif, and T. Esslinger, Experimental realization of the topological Haldane model with ultracold fermions, *Nature* **515**, 237 (2014).

[62] W. Zhao, K. Kang, Y. Zhang, P. Knüppel, Z. Tao, L. Li, C. L. Tschirhart, E. Redekop, K. Watanabe, T. Taniguchi, *et al.*, Realization of the Haldane Chern insulator in a moiré lattice, *Nat. Phys.* **20**, 275 (2024).

[63] S. Mitra, Á. Jiménez-Galán, M. Aulich, M. Neuhaus, R. E. Silva, V. Pervak, M. F. Kling, and S. Biswas, Light-wave-controlled Haldane model in monolayer hexagonal boron nitride, *Nature* **1** (2024).

[64] T. Oka and H. Aoki, Photovoltaic Hall effect in graphene, *Phys. Rev. B* **79**, 081406 (2009).

[65] J. W. McIver, B. Schulte, F.-U. Stein, T. Matsuyama, G. Jotzu, G. Meier, and A. Cavalleri, Light-induced anomalous Hall effect in graphene, *Nat. Phys.* **16**, 38 (2020).

[66] P. Zhou, G.-G. Liu, Y. Yang, Y.-H. Hu, S. Ma, H. Xue, Q. Wang, L. Deng, and B. Zhang, Observation of Photonic Antichiral Edge States, *Phys. Rev. Lett.* **125**, 263603 (2020).

[67] Y. Yang, D. Zhu, Z. Hang, and Y. Chong, Observation of antichiral edge states in a circuit lattice, *Sci. China Phys. Mech. Astron.* **64**, 1 (2021).

[68] J.-W. Liu, F.-L. Shi, K. Shen, X.-D. Chen, K. Chen, W.-J. Chen, and J.-W. Dong, Antichiral surface states in time-reversal-invariant photonic semimetals, *Nat. Commun.* **14**, 2027 (2023).

[69] X. Xi, B. Yan, L. Yang, Y. Meng, Z.-X. Zhu, J.-M. Chen, Z. Wang, P. Zhou, P. P. Shum, Y. Yang, *et al.*, Topological antichiral surface states in a magnetic Weyl photonic crystal, *Nat Commun* **14**, 1991 (2023).

[70] T. Frank, P. Högl, M. Gmitra, D. Kochan, and J. Fabian, Protected Pseudohelical Edge States in \mathbb{Z}_2 -Trivial Proximitized Graphene, *Phys. Rev. Lett.* **120**, 156402 (2018).

[71] X.-L. Lü and H. Xie, Bipolar and unipolar valley filter effects in graphene-based P/N junction, *New J. Phys.* **22**, 073003 (2020).

[72] S. A. Vitale, D. Nezich, J. O. Varghese, P. Kim, N. Gedik, P. Jarillo-Herrero, D. Xiao, and M. Rothschild, Valleytronics: Opportunities, Challenges, and Paths Forward, *Small* **14**, 1801483 (2018).

[73] T. D. Stanescu, V. Galitski, and S. Das Sarma, Topological states in two-dimensional optical lattices, *Phys. Rev. A* **82**, 013608 (2010).

[74] A. Raoux, M. Morigi, J.-N. Fuchs, F. Piéchon, and G. Montambaux, From Dia- to Paramagnetic Orbital Susceptibility of Massless Fermions, *Phys. Rev. Lett.* **112**, 026402 (2014).

[75] K. W. Lee, P.-H. Fu, and Y. S. Ang, Interplay between Haldane and modified Haldane models in $\alpha-T_3$ lattice: Band structures, phase diagrams, and edge states, *Phys. Rev. B* **109**, 235105 (2024).

[76] J. Vidal, R. Mosseri, and B. Douçot, Aharonov-Bohm Cages in Two-Dimensional Structures, *Phys. Rev. Lett.* **81**, 5888 (1998).

[77] J. Vidal, P. Butaud, B. Douçot, and R. Mosseri, Disorder and interactions in Aharonov-Bohm cages, *Phys. Rev. B* **64**, 155306 (2001).

[78] K. W. Lee, M. J. A. Calderon, X.-L. Yu, C. H. Lee, Y. S. Ang, and P.-H. Fu, Floquet engineering of topological phase transitions in quantum spin Hall $\alpha-T_3$ system (2024), [arXiv:2408.02093 \[cond-mat.mes-hall\]](https://arxiv.org/abs/2408.02093).

[79] N. Goldman and J. Dalibard, Periodically Driven Quantum Systems: Effective Hamiltonians and Engineered Gauge Fields, *Phys. Rev. X* **4**, 031027 (2014).

[80] S. Rahav, I. Gilary, and S. Fishman, Effective Hamiltonians for periodically driven systems, *Phys. Rev. A* **68**, 013820 (2003).

[81] R. Li, P.-H. Fu, J.-F. Liu, and J. Wang, Armchair edge states in shear-strained graphene: Magnetic properties and quantum valley Hall edge states, *Phys. Rev. B* **109**, 045403 (2024).

[82] C.-C. Liu, H. Jiang, and Y. Yao, Low-energy effective Hamiltonian involving spin-orbit coupling in silicene and two-dimensional germanium and tin, *Phys. Rev. B* **84**, 195430 (2011).

[83] X.-L. Lü, Y.-C. Zhang, P.-H. Fu, and J.-F. Liu, Phase diagrams and topological mixed edge states in silicene with intrinsic and extrinsic Rashba effects, *Phys. Rev. Res.* **6**, 043108 (2024).

[84] S.-Q. Lin, H. Tan, P.-H. Fu, and J.-F. Liu, Interaction-driven Chern insulating phases in the $\alpha-T_3$ lattice with Rashba spin-orbit coupling, *iScience* **26** (2023).

[85] X. Dai, P.-H. Fu, Y. S. Ang, and Q. Chen, Two-dimensional Weyl nodal-line semimetal and antihelical edge states in a modified Kane-Mele model, *Phys. Rev. B* **110**, 195409 (2024).